

Supporting Information

Dual-Metal Single-Atoms with Dual-coordination for the Domino Synthesis of Natural Flavones

Xin Zhao¹, Ruiqi Fang^{1,*}, Fengliang Wang¹, Xiangpeng Kong², Yingwei Li^{1,3,*}

¹School of Chemistry and Chemical Engineering, South China University of Technology, Guangzhou 510640, China

²The School of Materials Science and Engineering, Harbin Institute of Technology, Shenzhen 518055, China

³ State Key Laboratory of Pulp and Paper Engineering, South China University of Technology, Guangzhou 510640, China

Email: fangrq@scut.edu.cn; liyw@scut.edu.cn

Experimental

Chemicals

All chemicals were purchased from commercial sources and directly used without further purification. Zinc acetate dihydrate ($\text{Zn}(\text{OAc})_2 \cdot 2\text{H}_2\text{O}$, 99.99%, Aladdin), copper acetate monohydrate ($\text{Cu}(\text{OAc})_2 \cdot \text{H}_2\text{O}$, 99%, Aladdin), cobalt acetate tetrahydrate ($\text{Co}(\text{OAc})_2 \cdot 4\text{H}_2\text{O}$, 99.99%, Aladdin), 2-methylimidazole (2-MI, 98%, Aladdin), iron chloride hexahydrate ($\text{FeCl}_3 \cdot 6\text{H}_2\text{O}$, 99%, Aladdin), nickel nitrate hexahydrate ($\text{Ni}(\text{NO}_3)_2 \cdot 6\text{H}_2\text{O}$, 99%, Aladdin), manganese sulfate monohydrate ($\text{MnSO}_4 \cdot \text{H}_2\text{O}$, 98%, Aladdin), sodium tetrachloroaurate dihydrate ($\text{NaAuCl}_4 \cdot 2\text{H}_2\text{O}$, Aladdin), potassium tetrachloroplatinate (K_2PtCl_4 , 98%, Aladdin), potassium tetrachloropalladate (K_2PdCl_4 , 98%, Aladdin), melamine (99%, Aladdin), phytic acid (50% in H_2O , Aladdin).

Synthesis of hollow Cu-complex@MP'-Co precursors and $\text{CuN}_4/\text{CoN}_3\text{P}_1$ @NPC nano-dodecahedrons

The Cu-complex@MP'-Co was synthesized by using the same recipes as Cu-complex@MP-Co except for the usage of phytic acid (0.050 g).

Typically, the as-prepared Cu-complex@MP'-Co was placed in a tubular furnace, which was heated to 600 °C using a ramp rate of 1 °C min⁻¹ and kept for 120 min, and then heated to 700 °C using a ramp rate of 2 °C min⁻¹ under Ar atmosphere to obtain $\text{CuN}_4/\text{CoN}_3\text{P}_1$ @NPC nano-dodecahedrons.

Synthesis of hollow Cu-complex@PA-Co precursors and $\text{CuN}_4/\text{CoN}_4$ @NPC nano-

dodecahedrons

The Cu-complex@PA-Co was synthesized by using the same recipes as Cu-complex@MP-Co except for replacing aqueous solution of melamine with deionized water.

Typically, the as-prepared Cu-complex@PA-Co was placed in a tubular furnace, which was heated to 600 °C using a ramp rate of 1 °C min⁻¹ and kept for 120 min, and then heated to 700 °C using a ramp rate of 2 °C min⁻¹ under Ar atmosphere to obtain CuN₄/CoN₄@NPC nano-dodecahedrons.

Synthesis of Cu-complex@MP-M and Co-complex@MP-M precursors and corresponding CuN₄/MN_xP_y@NPC and CoN₄/MN_xP_y@NPC

The Cu-complex@MP-M and Co-complex@MP-M were synthesized by using the same recipes as Cu-complex@MP-Co except for the metal species (Fe³⁺, Ni²⁺, Mn²⁺, Au³⁺, Pt²⁺, and Pd²⁺, respectively).

The as-synthesized Cu-complex@MP-M and Co-complex@MP-M was placed in a tubular furnace, which was heated to 600 °C using a ramp rate of 1 °C min⁻¹ and kept for 120 min, and then heated to 700 °C using a ramp rate of 2 °C min⁻¹ under Ar atmosphere to obtain CuN₄/FeN_xP_y@NPC, CuN₄/NiN_xP_y@NPC, CuN₄/MnN_xP_y@NPC, CuN₄/AuN_xP_y@NPC, CuN₄/PtN_xP_y@NPC, CuN₄/PdN_xP_y@NPC, CoN₄/FeN_xP_y@NPC, CoN₄/NiN_xP_y@NPC, CoN₄/MnN_xP_y@NPC, CoN₄/AuN_xP_y@NPC, CoN₄/PtN_xP_y@NPC, and CoN₄/PdN_xP_y@NPC, respectively.

Synthesis of Cu-complex@MP and Cu-complex@MP-700

The Cu-complex@MP was synthesized by using the same recipes as Cu-complex@MP-Co except for no $\text{Co}(\text{NO}_3)_2 \cdot 6\text{H}_2\text{O}$ was added.

The as-synthesized Cu-complex@MP was heated to 600 °C using a ramp rate of 1 °C min⁻¹ and kept for 120 min, and then heated to 700 °C using a ramp rate of 2 °C min⁻¹ under Ar atmosphere to obtain Cu-complex@MP-700.

Synthesis of MP-Co-700 and MP-700

Typically, 1 mL aqueous solution containing $\text{Co}(\text{NO}_3)_2 \cdot 6\text{H}_2\text{O}$ (0.005 g) and phytic acid (0.065 g) was added to the aqueous solution of melamine (0.016 M, 50 mL) under vigorous stirring for 30 min at room temperature. The obtained light pink powders were heated to 600 °C using a ramp rate of 1 °C min⁻¹ and kept for 120 min, and then heated to 700 °C using a ramp rate of 2 °C min⁻¹ under Ar atmosphere to obtain MP-Co-700.

The MP-700 was synthesized by using the same recipes as MP-Co-700 except for no $\text{Co}(\text{NO}_3)_2 \cdot 6\text{H}_2\text{O}$ was added.

Materials characterization

The size and morphology of materials were studied by scanning electron microscopy (SEM) and transmission electron microscopy (TEM). SEM was carried out on a JEOL-6700 instrument. TEM was recorded on JEM-2100F. High-angle annular dark-field scanning transmission electron microscopy (HAADF-STEM), spherical

aberration correction HAADF-STEM (AC HAADF-STEM), and annular bright field scanning TEM (ABF-STEM) were recorded on a FEI Titan Cubed Themis G2 300 S/TEM with a probe corrector and a monochromator at 200 kV. Powder X-ray diffraction (PXRD) patterns of the samples were obtained on a Rigaku diffractometer (D/max-III A, 3 kW) with Cu K α radiation ($\lambda = 1.5406 \text{ \AA}$) at a voltage of 40 kV and a current of 10 mA at room temperature. Brunauer-Emmett-Teller (BET) surface area and pore size measurements were performed on a Micromeritics ASAP 2020M instrument at 77 K. Before the analysis, the samples were degassed at 150 °C for 12 hours. X-ray photoelectron spectroscopy (XPS) was collected on a Thermo Scientific K-Alpha system with the C 1s peak (284.6 eV) as reference. The metal contents of the samples were determined by ICP-OES on an Optima 8300 instrument. Thermogravimetric analysis (TGA) was performed on a NETZSCH STA449C instrument loaded with 5 mg sample using a heating rate of 5 °C/min under argon atmosphere. The N elemental contents of the samples were measured on a Euro Vector EA3000 instrument (EA).

The X-ray absorption experiments were carried out at the XAS station (BL14W1) of the Shanghai Synchrotron Radiation Facility (SSRF). The electron storage ring was operated at 3.5 GeV. Si (311) double-crystal was used as the monochromator, and the data was collected using solid-state detector under ambient conditions. The beam size was limited by the horizontal and vertical slits with the area of $1 \times 4 \text{ mm}^2$ during XAS measurements.

Calculation details

Spin-polarized density functional theory (DFT) calculations were performed with the Vienna ab initio simulation package (VASP), using projector augmented wave (PAW) pseudopotential for the core electrons, a cutoff energy (450 eV) for the valence electrons, and the generalized gradient approximation (GGA) in the form of Perdew-Burke-Ernzerhof (PBE) for the exchange correlation potentials. All models were constructed based on a rectangle graphene supercell with lattice constants a and b as 12.78 and 12.30 Å, containing 60 carbon atoms. To avoid interactions between adjacent images the c axis of these models is set to be 20 Å. The atoms were relaxed fully until the energy convergence reaches 0.00001 eV and the force acting on each atom was less than 0.01 eV/Å. The lattice constants of all models are relaxed, as well. Van der Waals interaction was considered at the DFT-D2 level as proposed by Grimme.

DFT for O₂ activation and dissociation: The transition states are located via the climbing image nudged elastic band (CI-NEB) method.

DFT for the reaction: spin-polarized DFT calculations were performed using the Vienna ab initio simulation package (VASP). The generalized gradient approximation proposed by Perdew, Burke, and Ernzerhof (GGA-PBE) is selected for the exchange-correlation potential. The pseudo-potential was described by the projector-augmented-wave (PAW) method. The geometry optimization is performed until the Hellmann-Feynman force on each atom is smaller than 0.03 eV·Å⁻¹. The energy criterion is set to 10⁻⁶ eV in iterative solution of the Kohn-Sham equation. Dimer method is used to find the transition states.

Domino synthesis of flavone

The domino reaction of benzyl alcohol and 2'-hydroxyacetophenone was carried out in a high-pressure reactor with a magnetic stirrer. In a typical run, benzyl alcohol (1 mmol), 2'-hydroxyacetophenone (1.5 mmol), catalyst (total metals, 2 mol% relative to benzyl alcohol), K₂CO₃ (0.2 mmol), *n*-hexanol (4 mL) were sealed in a high-pressure reactor (NSG25-P5-T3-SS1-SV, Anhui Kemi Machinery Technology Co., Ltd). The high-pressure reactor was evacuated, refilled with 2 bar O₂, and heated to 120 °C for 12 h under magnetic stirring. After reaction, the reactor was cooled to room temperature. The catalyst was isolated from the solution by centrifugation and directly reused after washing and drying. The products were quantified by a GC-MS spectrometer (Agilent, 7890B GC/5977A MS) equipped with a DB-35 MS UI capillary column (0.25 mm × 30 m). The products were also confirmed by nuclear magnetic resonance (NMR) analysis.

The conversion and selectivity were calculated using the following equations:

$$\text{Benzyl alcohol conversion} = \left(1 - \frac{\text{Moles of benzyl alcohol}}{\text{Moles of benzyl alcohol loaded}} \right) \times 100\%$$

$$\text{Flavone selectivity} = \left(\frac{\text{Moles of flavone}}{\text{Moles of benzyl alcohol converted}} \right) \times 100\%$$

$$\text{Flavone yield} = \left(\frac{\text{Moles of flavone}}{\text{Moles of benzyl alcohol loaded}} \right) \times 100\%$$

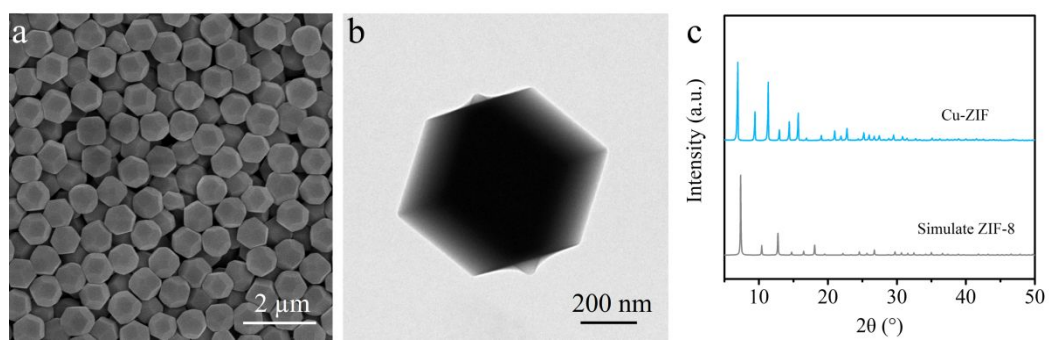


Figure S1. (a) SEM, (b) TEM images, (c) XRD pattern of the as-synthesized Cu-ZIF.

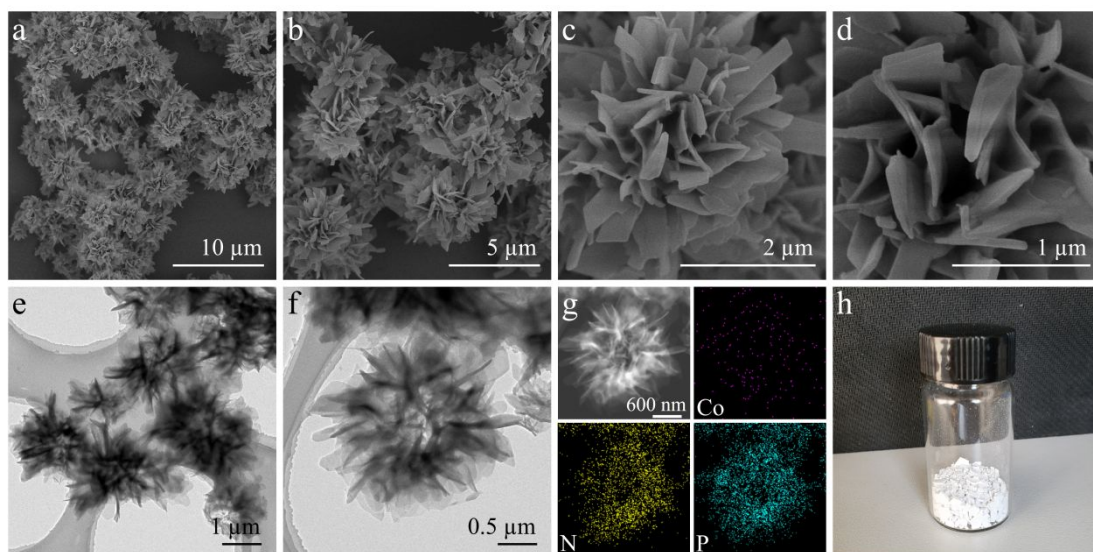


Figure S2. (a-d) SEM, (e, f) TEM, (g) HAADF-STEM and corresponding elemental mapping images, (h) optical image of the as-synthesized MP-Co.

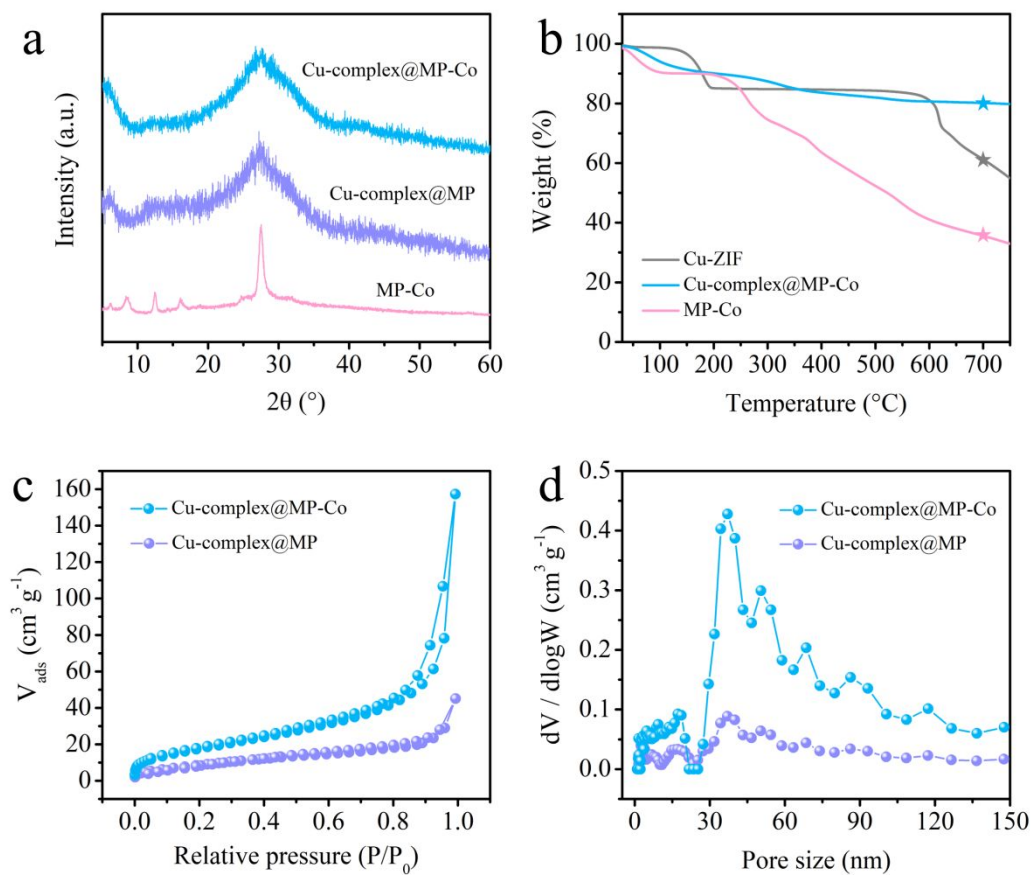


Figure S3. (a) XRD patterns of Cu-complex@MP-Co, Cu-complex@MP, and MP-Co. (b) TG curves of Cu-ZIF, Cu-complex@MP-Co, and MP-Co. (c) N_2 adsorption-desorption isotherms, and (d) corresponding pore-size distributions of Cu-complex@MP and Cu-complex@MP-Co.

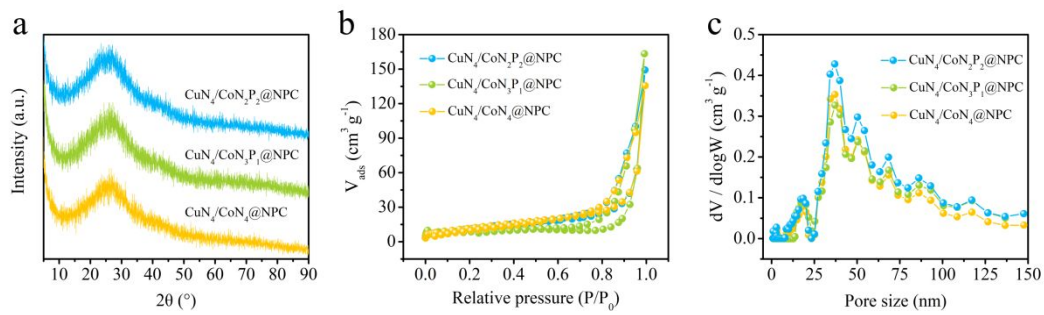


Figure S4. (a) XRD patterns, (b) N₂ adsorption-desorption isotherms, and (c) corresponding pore-size distributions of CuN₄/CoN₂P₂@NPC, CuN₄/CoN₃P₁@NPC, and CuN₄/CoN₄@NPC.

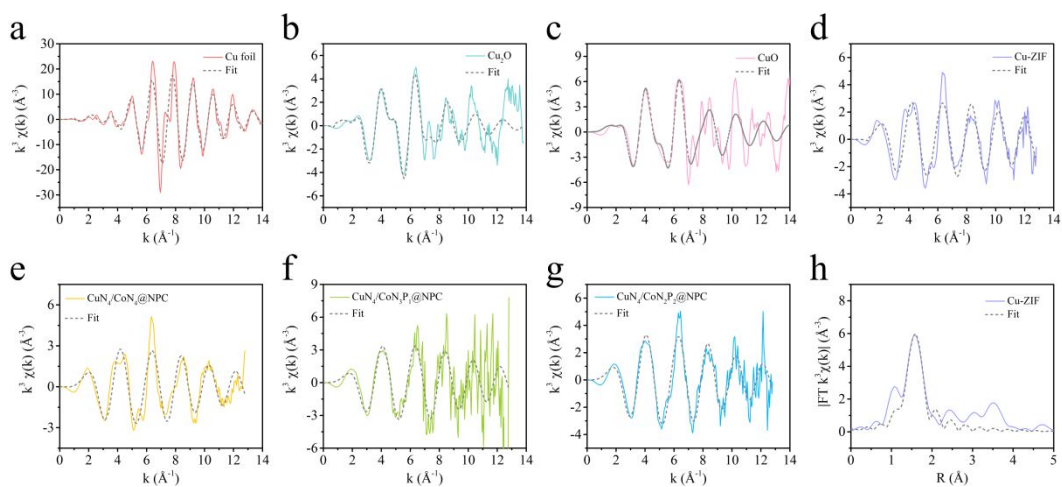


Figure S5. Cu K-edge EXAFS fitting curves of (a) Cu foil, (b) Cu_2O , (c) CuO , (d) Cu-ZIF, (e) $\text{CuN}_4/\text{CoN}_4@\text{NPC}$, (f) $\text{CuN}_4/\text{CoN}_3\text{P}_1@\text{NPC}$, (g) $\text{CuN}_4/\text{CoN}_2\text{P}_2@\text{NPC}$. (h) The corresponding EXAFS fitting curves of Cu-ZIF in R space.

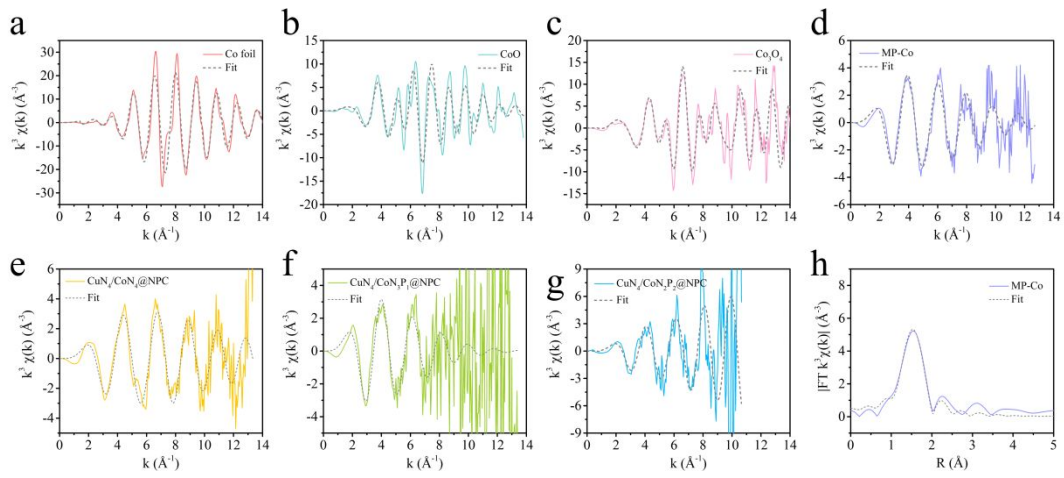


Figure S6. Co K-edge EXAFS fitting curves of (a) Co foil, (b) CoO, (c) Co₃O₄, (d) MP-Co, (e) CuN₄/CoN₄@NPC, (f) CuN₄/CoN₃P₁@NPC, (g) CuN₄/CoN₂P₂@NPC. (h) The corresponding EXAFS fitting curves of MP-Co in R space.

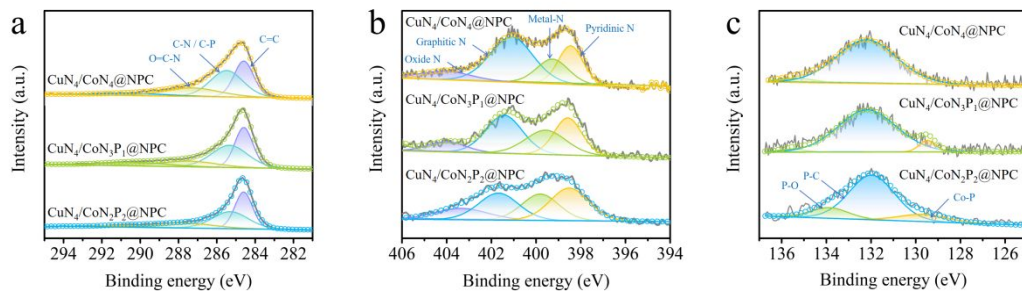


Figure S7. XPS spectra in (a) C 1s region, (b) N 1s region, and (c) P 2p region of $\text{CuN}_4/\text{CoN}_2\text{P}_2@\text{NPC}$, $\text{CuN}_4/\text{CoN}_3\text{P}_1@\text{NPC}$, and $\text{CuN}_4/\text{CoN}_4@\text{NPC}$.

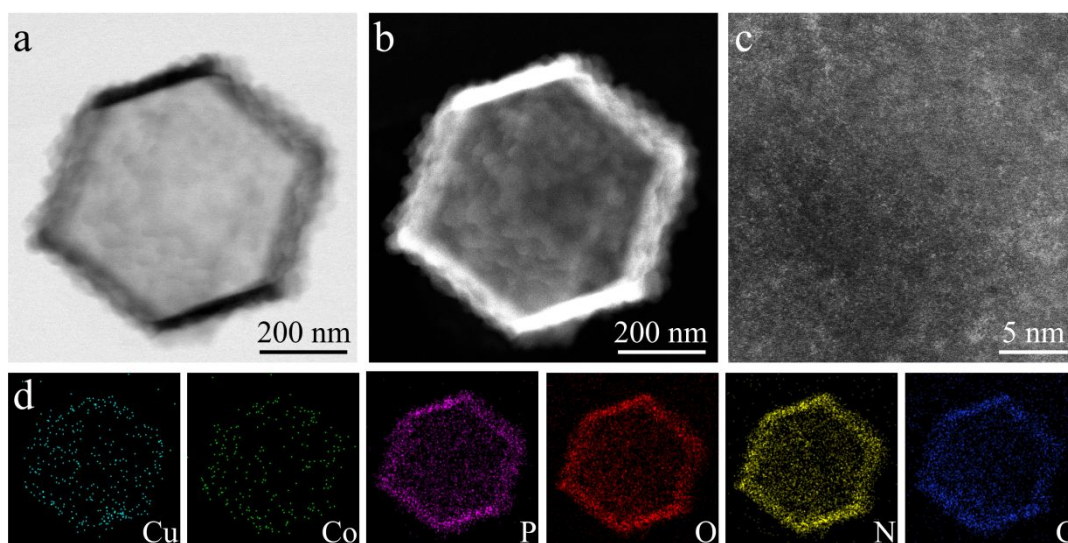


Figure S8. (a) ABF-STEM, (b) HAADF-STEM, (c) AC HAADF-STEM, and (d) corresponding elemental mapping images of the as-synthesized $\text{CuN}_4/\text{CoN}_3\text{P}_1@\text{NPC}$.

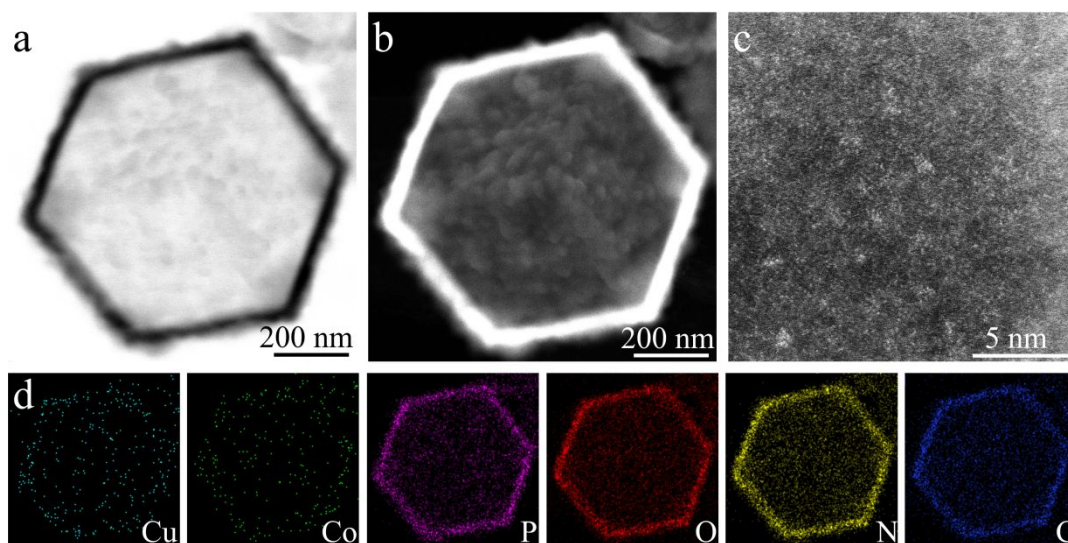


Figure S9. (a) ABF-STEM, (b) HAADF-STEM, (c) AC HAADF-STEM, and (d) corresponding elemental mapping images of the as-synthesized $\text{CuN}_4/\text{CoN}_4@\text{NPC}$.

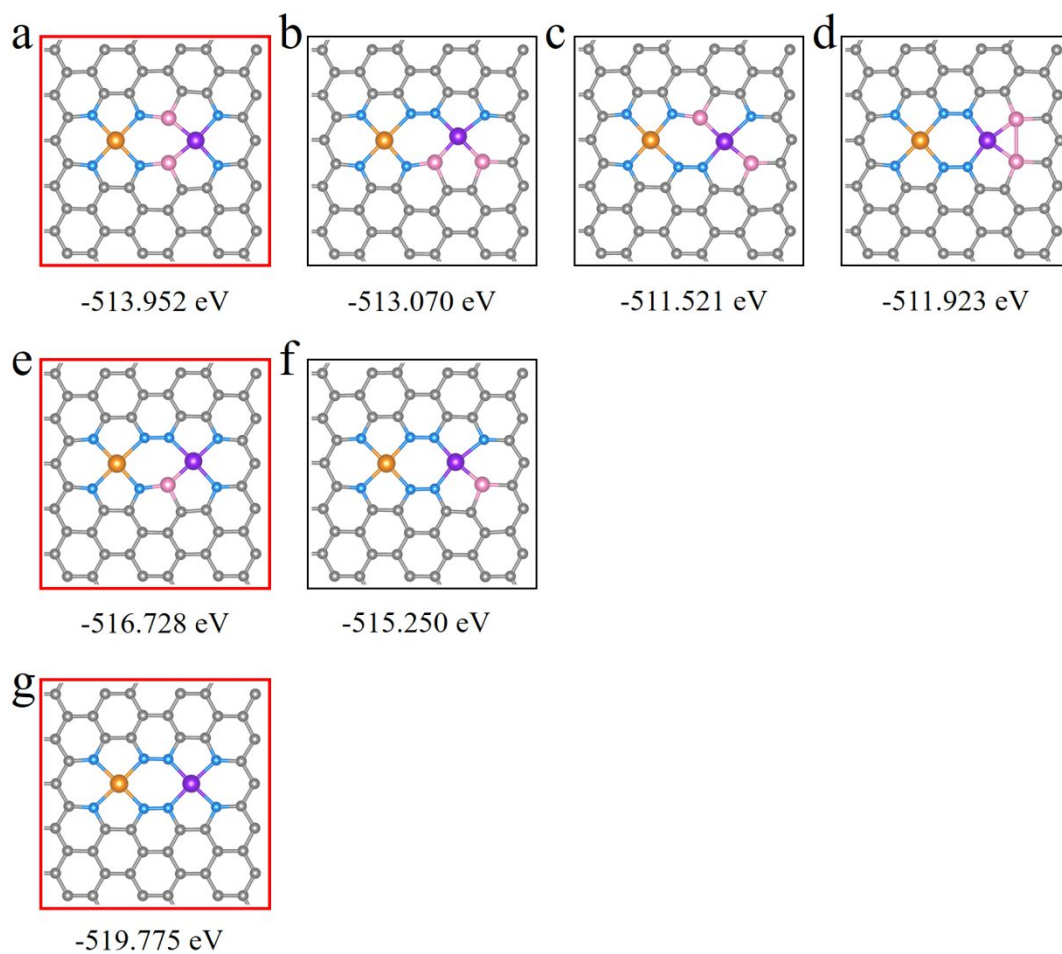


Figure S10. The proposed models of (a-d) CuN₄/CoN₂P₂@NPC, (e-f) CuN₄/CoN₃P₁@NPC, (g) CuN₄/CoN₄@NPC. C (gray), N (blue), P (pink), Cu (orange), and Co (purple).

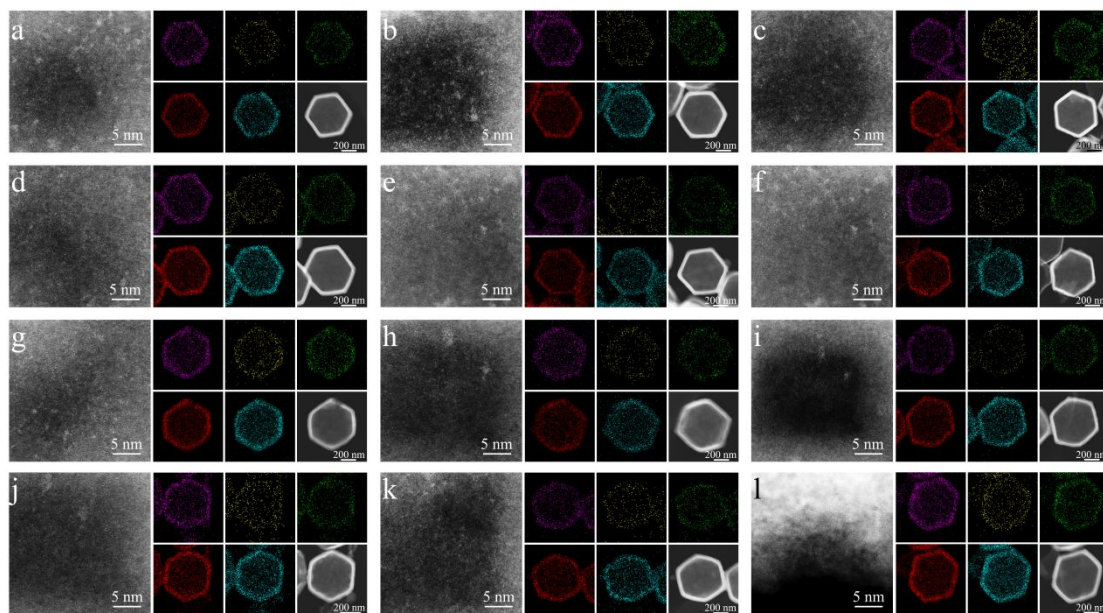


Figure S11. AC HAADF-STEM, HAADF-STEM, and corresponding elemental mapping images of (a) $\text{CuN}_4/\text{FeN}_x\text{P}_y@\text{NPC}$, (b) $\text{CuN}_4/\text{NiN}_x\text{P}_y@\text{NPC}$, (c) $\text{CuN}_4/\text{MnN}_x\text{P}_y@\text{NPC}$, (d) $\text{CuN}_4/\text{AuN}_x\text{P}_y@\text{NPC}$, (e) $\text{CuN}_4/\text{PtN}_x\text{P}_y@\text{NPC}$, (f) $\text{CuN}_4/\text{PdN}_x\text{P}_y@\text{NPC}$, (g) $\text{CoN}_4/\text{FeN}_x\text{P}_y@\text{NPC}$, (h) $\text{CoN}_4/\text{NiN}_x\text{P}_y@\text{NPC}$, (i) $\text{CoN}_4/\text{MnN}_x\text{P}_y@\text{NPC}$, (j) $\text{CoN}_4/\text{AuN}_x\text{P}_y@\text{NPC}$, (k) $\text{CoN}_4/\text{PtN}_x\text{P}_y@\text{NPC}$, (l) $\text{CoN}_4/\text{PdN}_x\text{P}_y@\text{NPC}$.

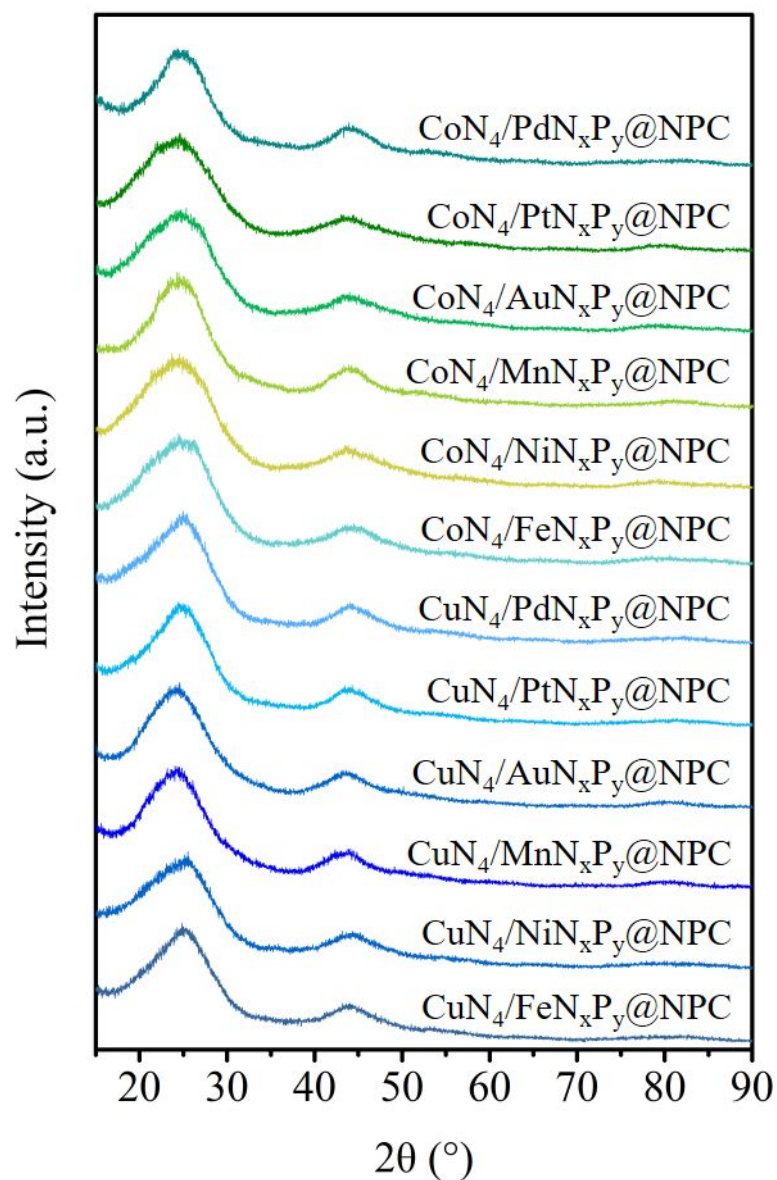


Figure S12. XRD patterns of the as-synthesized $\text{CuN}_4/\text{FeN}_x\text{P}_y@\text{NPC}$, $\text{CuN}_4/\text{NiN}_x\text{P}_y@\text{NPC}$, $\text{CuN}_4/\text{MnN}_x\text{P}_y@\text{NPC}$, $\text{CuN}_4/\text{AuN}_x\text{P}_y@\text{NPC}$, $\text{CuN}_4/\text{PtN}_x\text{P}_y@\text{NPC}$, $\text{CuN}_4/\text{PdN}_x\text{P}_y@\text{NPC}$, $\text{CoN}_4/\text{FeN}_x\text{P}_y@\text{NPC}$, $\text{CoN}_4/\text{NiN}_x\text{P}_y@\text{NPC}$, $\text{CoN}_4/\text{MnN}_x\text{P}_y@\text{NPC}$, $\text{CoN}_4/\text{AuN}_x\text{P}_y@\text{NPC}$, $\text{CoN}_4/\text{PtN}_x\text{P}_y@\text{NPC}$, $\text{CoN}_4/\text{PdN}_x\text{P}_y@\text{NPC}$.

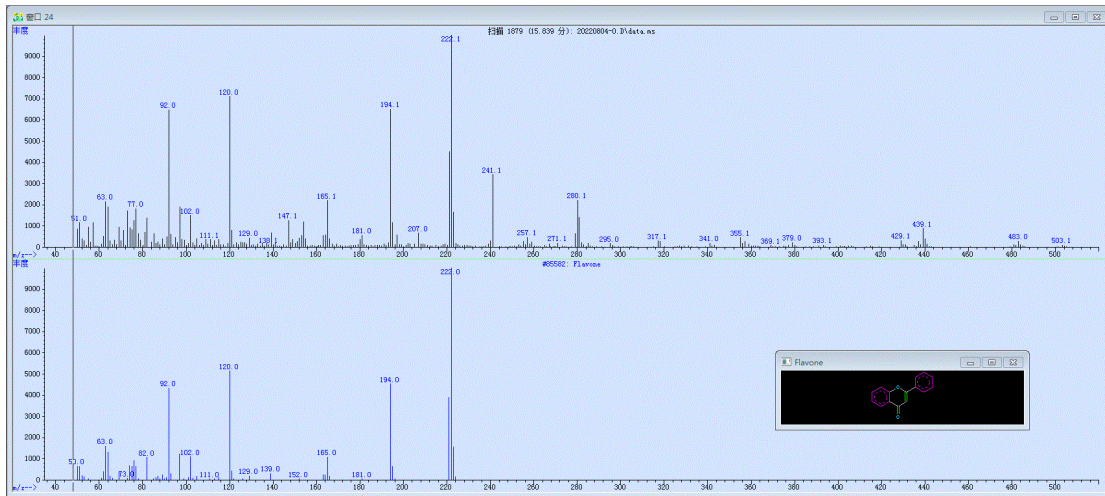


Figure S13. A typical GC-MS spectra of the as-synthesized flavone.

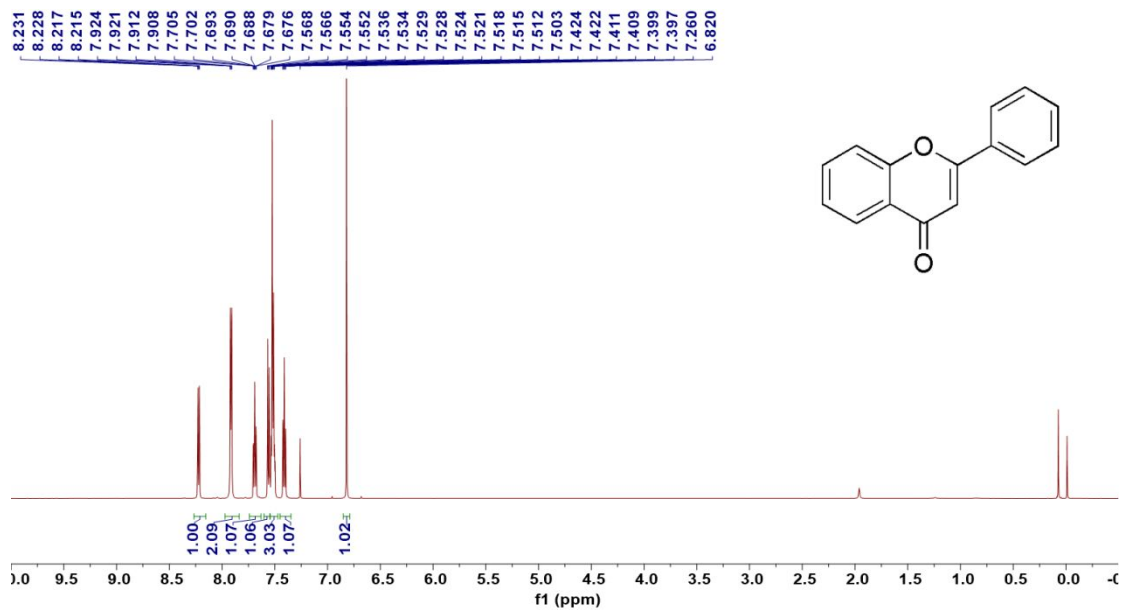


Figure S14. $^1\text{H-NMR}$ spectrum of the as-synthesized flavone.

$^1\text{H-NMR}$ (600 MHz, Chloroform- d) δ 8.22 (dd, $J = 7.9, 1.7$ Hz, 1H), 7.92 (dd, $J = 7.8, 1.9$ Hz, 2H), 7.69 (ddd, $J = 8.7, 7.1, 1.7$ Hz, 1H), 7.56 (dd, $J = 8.4, 1.0$ Hz, 1H), 7.54 – 7.47 (m, 3H), 7.41 (td, $J = 7.5, 7.1, 1.1$ Hz, 1H), 6.82 (s, 1H).

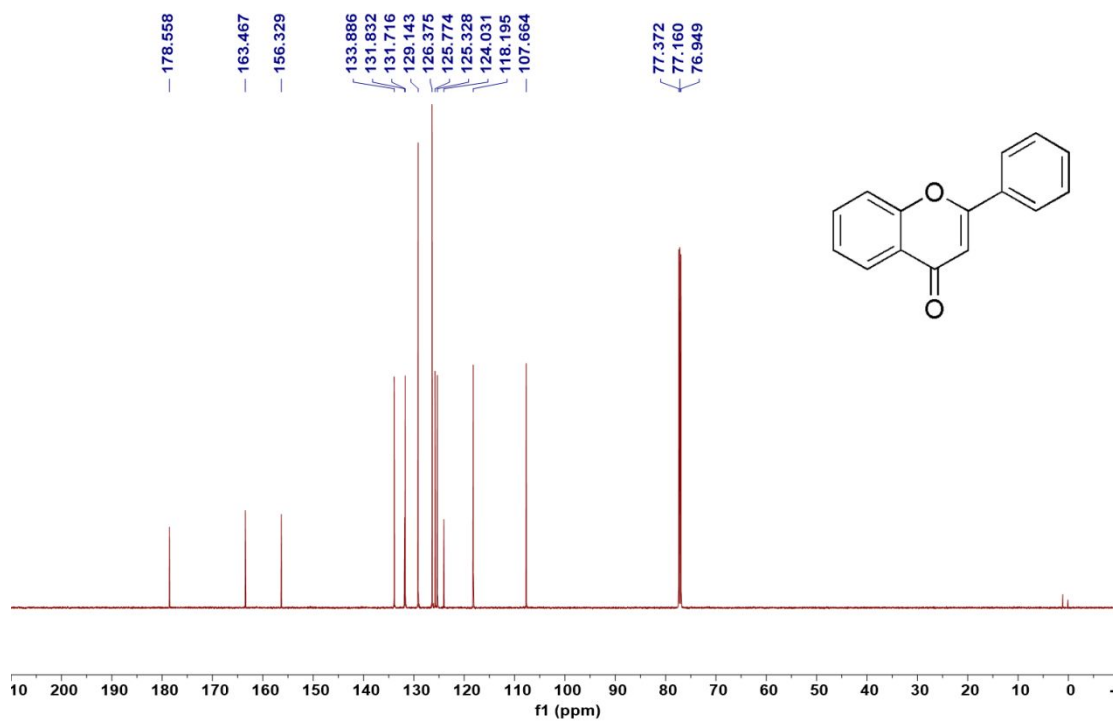


Figure S15. ¹³C-NMR spectrum of the as-synthesized flavone.

¹³C-NMR (151 MHz, Chloroform-d) δ 178.56, 163.47, 156.33, 133.89, 131.83, 131.72, 129.14, 126.38, 125.77, 125.33, 124.03, 118.19, 107.66.

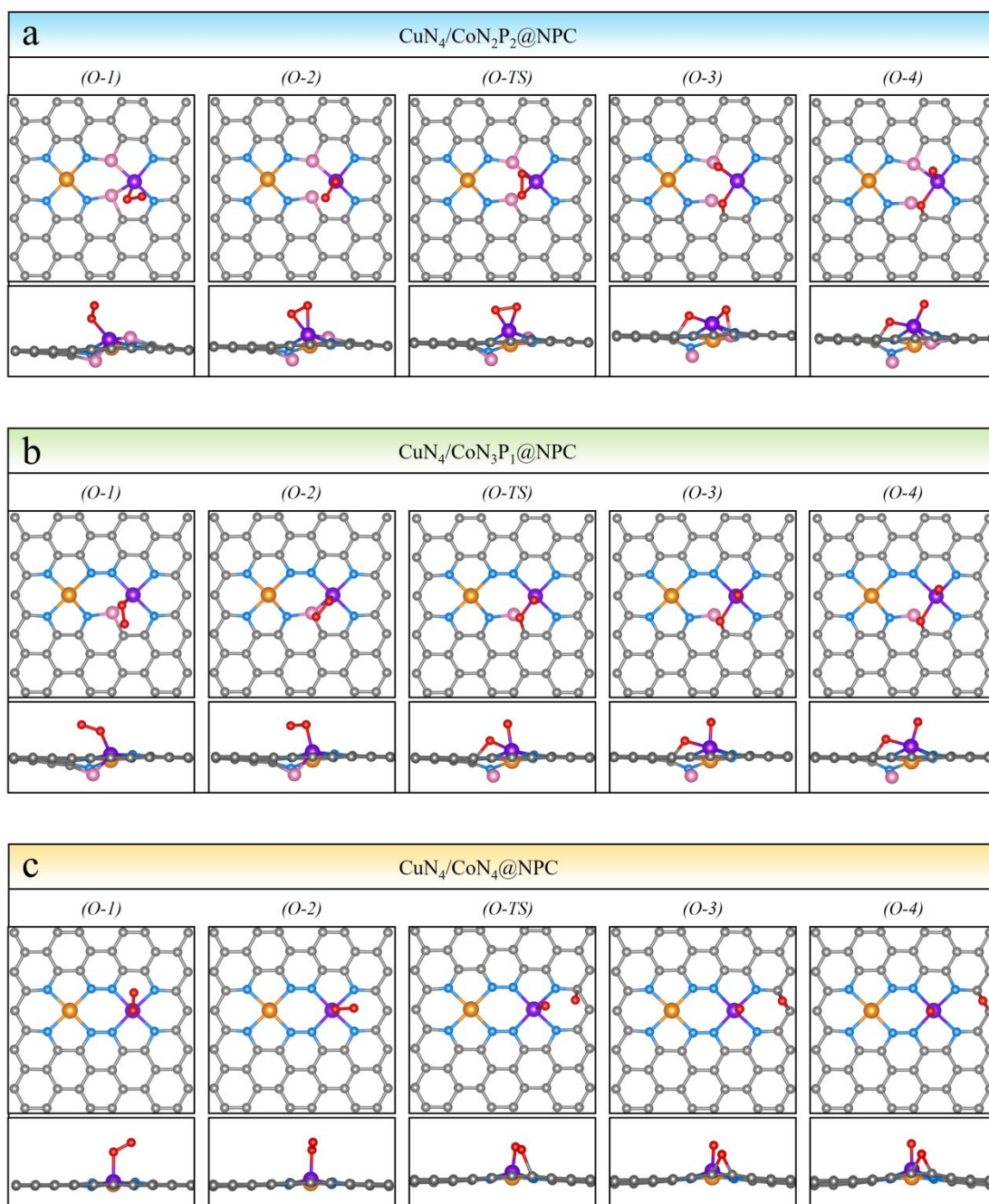


Figure S16. Top and side view of the atomistic structure of the initial state, transition state, and final state for the O_2 adsorption, disassociation, and activation over (a) $\text{CuN}_4/\text{CoN}_2\text{P}_2@\text{NPC}$, (b) $\text{CuN}_4/\text{CoN}_3\text{P}_1@\text{NPC}$, and (c) $\text{CuN}_4/\text{CoN}_4@\text{NPC}$. The gray, blue, pink, orange, purple, and red balls represent C, N, P, Cu, Co, and O atoms, respectively. “TS” denotes a transition state.

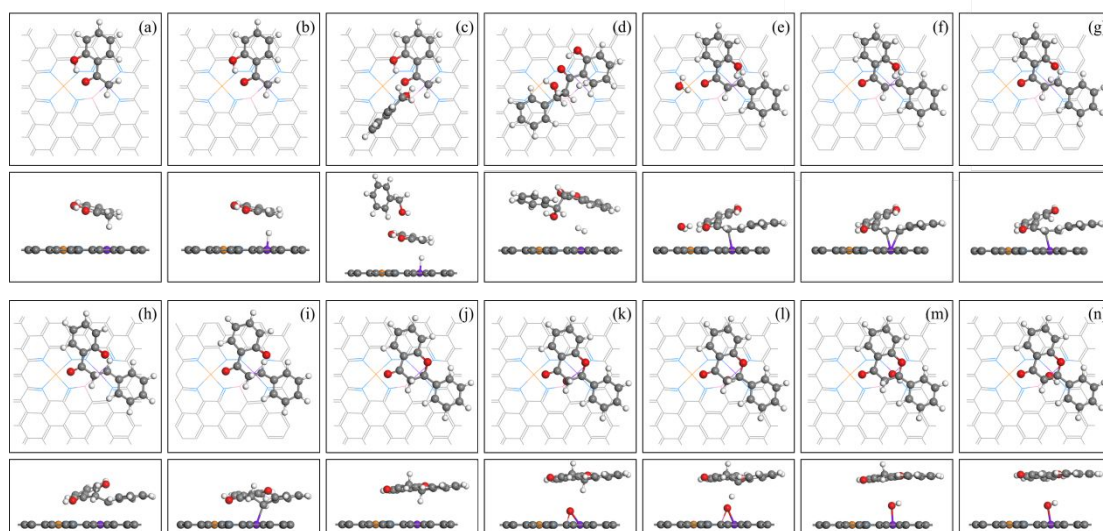


Figure S17. TOP (the catalyst substrate is simplified into a linear structure) and side view of the atomistic structure for the reaction pathways from benzyl alcohol and 2'-hydroxyacetophenone to flavone on $\text{CuN}_4/\text{CoN}_3\text{P}_1@\text{NPC}$. The orange, purple, gray, blue, red, pink, and white balls represent Cu, Co, C, N, O, P, and H atoms, respectively. “TS” denotes a transition state.

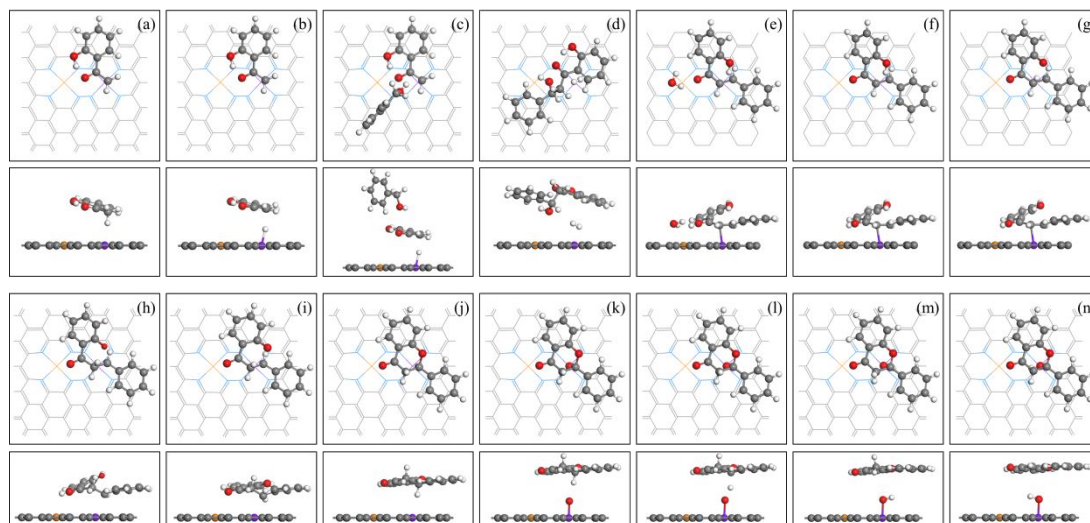


Figure S18. TOP (the catalyst substrate is simplified into a linear structure) and side view of the atomistic structure for the reaction pathways from benzyl alcohol and 2'-hydroxyacetophenone to flavone on CuN₄/CoN₄@NPC. The orange, purple, gray, blue, red, pink, and white balls represent Cu, Co, C, N, O, P, and H atoms, respectively. “TS” denotes a transition state.

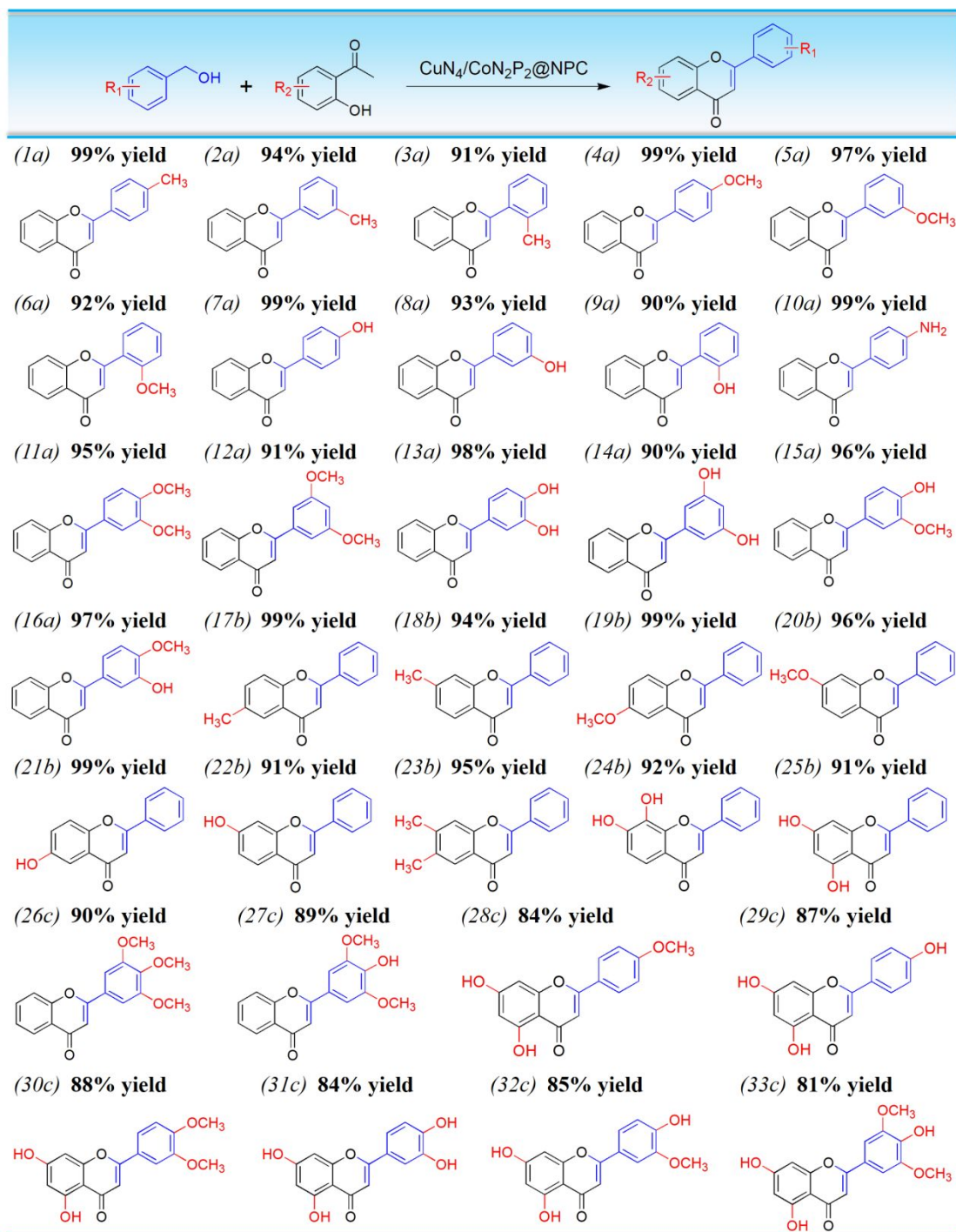


Figure S19. Substrate scope of oxidative coupling-dehydrogenation cascade reaction over $\text{CuN}_4/\text{CoN}_2\text{P}_2@\text{NPC}$.

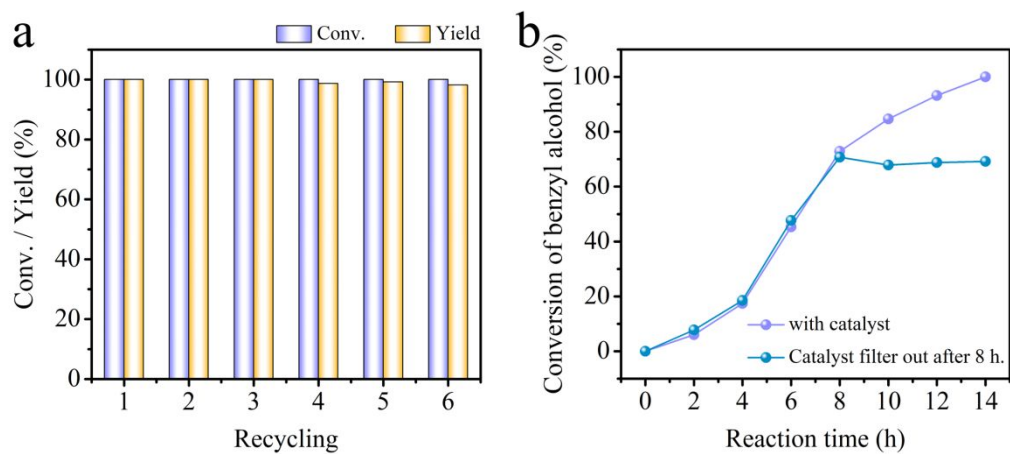


Figure S20. (a) Reusability results of the $\text{CuN}_4/\text{CoN}_2\text{P}_2@\text{NPC}$ catalyst in the synthesis of flavone. (b) The hot filtration experiment results over $\text{CuN}_4/\text{CoN}_2\text{P}_2@\text{NPC}$.

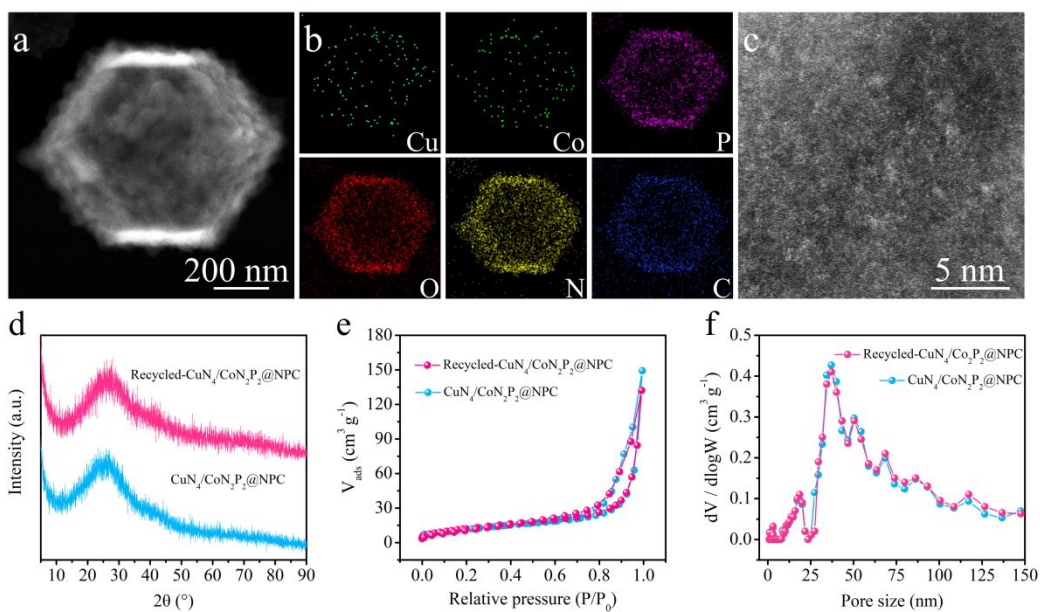


Figure S21. (a) HAADF-STEM, (b) corresponding elemental mapping, and (c) AC HAADF-STEM images of the recycled $\text{CuN}_4/\text{CoN}_2\text{P}_2@\text{NPC}$. (d) XRD patterns, (e) N_2 adsorption-desorption isotherms, (f) corresponding pore-size distributions of the fresh and recycled $\text{CuN}_4/\text{CoN}_2\text{P}_2@\text{NPC}$.

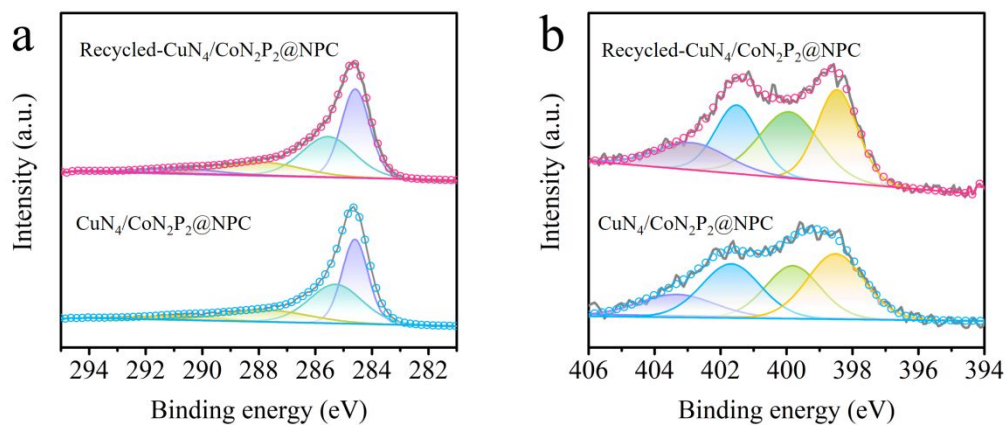


Figure S22. (a) C 1s region, (b) N 1s region of the fresh and recycled $\text{CuN}_4/\text{CoN}_2\text{P}_2@\text{NPC}$.

Table S1. Characterization results of the as-prepared samples.

Sample	S_{BET} ($\text{m}^2 \text{g}^{-1}$)	Pore volume ($\text{cm}^3 \text{g}^{-1}$)	Elemental contents (wt%)			
			N	P	Cu	Co
CuN ₄ /CoN ₂ P ₂ @NPC	42.9	0.18	6.0	12.1	1.6	1.1
CuN ₄ /CoN ₃ P ₁ @NPC	40.6	0.16	5.2	10.7	1.7	1.2
CuN ₄ /CoN ₄ @NPC	44.5	0.15	3.8	7.5	1.9	1.8
Recycled CuN ₄ /CoN ₂ P ₂ @NPC	44.2	0.19	6.1	11.9	1.5	1.1

Table S2. Structural parameters of various samples extracted from the EXAFS fitting ($S_0^2=0.91$).

Sample	Path	C.N.	R (Å)	$\sigma^2 \times 10^3$ (Å ²)	ΔE (eV)	R factor
Cu foil	Cu-Cu	12*	2.54±0.01	8.6±0.2	6.3±0.4	0.002
Cu ₂ O	Cu-O	3.2±0.4	1.92±0.01	7.2±1.3	0.2±1.3	0.009
	Cu-Cu	11.5±3.2	3.02±0.02	32.7±3.6	2.2±1.4	
CuO	Cu-O	4.1±0.8	1.95±0.01	5.1±2.1	1.0±2.0	0.019
	Cu-Cu	12.1±2.6	2.97±0.04	33.2±8.4	0.0±3.4	
Zn/Cu-ZIF	Cu-N	3.0±0.7	1.99±0.01	2.8±1.7	5.5±3.3	0.016
CuN ₄ /CoN ₄ @NPC	Cu-N	3.5±0.8	1.97±0.01	4.6±1.9	2.3±3.2	0.018
	Cu-N	4.6±0.8	1.96±0.01	4.6±1.5	-2.8±2.0	0.009
CuN ₄ /CoN ₃ P ₁ @NPC	Cu-N	4.6±0.8	1.96±0.01	4.6±1.5	-2.8±2.0	0.009
CuN ₄ /CoN ₂ P ₂ @NPC	Cu-N	4.8±0.5	1.97±0.01	5.5±0.8	-2.0±1.4	0.003

[^a] C.N.: coordination numbers; [^b] R: bond distance; [^c] σ^2 : Debye-Waller factors; [^d] ΔE : the inner potential correction. R factor: goodness of fit. * Fitting with fixed parameter.

Table S3. Structural parameters of various samples extracted from the EXAFS fitting ($S_0^2=0.83$).

Sample	Path	C.N.	R (Å)	$\sigma^2 \times 10^3$ (Å ²)	ΔE (eV)	R factor
Co foil	Co-Co	12*	2.49±0.01	6.3±0.1	8.3±0.3	0.001
CoO	Co-O	5.7±0.9	2.11±0.01	8.5±1.3	0.2±1.7	0.004
	Co-Co	12.5±1.5	3.01±0.01	9.7±1.0	-3.2±1.1	
	Co-O	4.2±0.4	1.92±0.01	1.9±0.8	2.3±1.3	
Co ₃ O ₄	Co-Co	4.4±1.8	2.88±0.02	4.1±2.6	2.5±3.2	0.006
	Co-O	5.0±2.6	3.34±0.02	3.2±3.0	-2.8±3.4	
MP-Co	Co-N	6.8±1.1	2.07±0.01	8.5±2.0	1.2±1.6	0.009
CuN ₄ /CoN ₂ P ₂ @NPC	Co-N	2*	1.95±0.06	5.2±1.7	-10.4±4.2	0.019
	Co-P	2*	2.26±0.03			
CuN ₄ /CoN ₃ P ₁ @NPC	Co-N	3*	2.00±0.04	3.3±1.4	-3.5±3.9	0.017
	Co-P	1*	2.30±0.04			
CuN ₄ /CoN ₄ @ NPC	Co-N	4.4±0.5	1.88±0.01	3.9±0.8	-6.0±1.4	0.003

[^a] C.N.: coordination numbers; [^b] R: bond distance; [^c] σ^2 : Debye-Waller factors; [^d] ΔE : the inner potential correction. R factor: goodness of fit. * Fitting with fixed parameter.

Table S4. Bader charge analysis of the models.

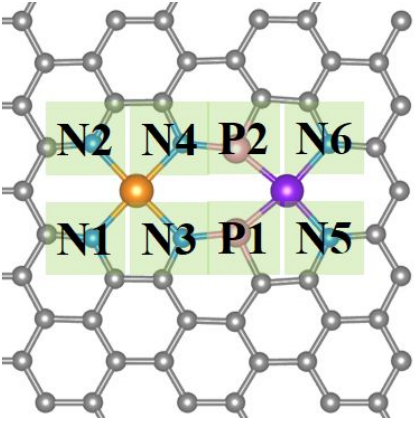
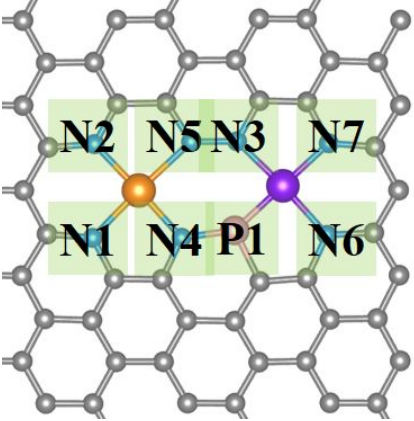
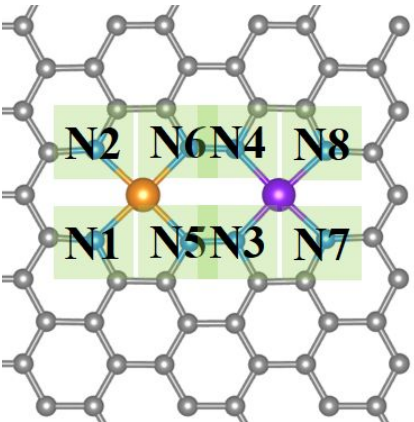
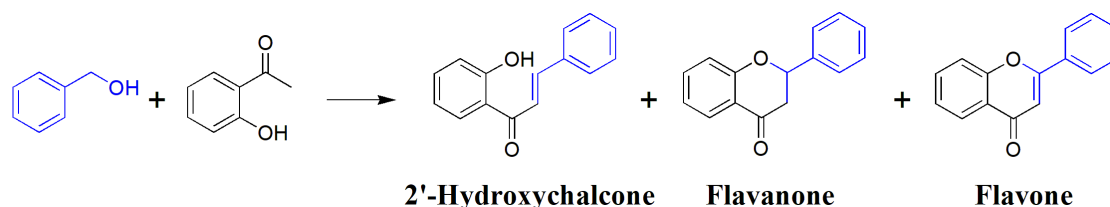
Sample	Atom	Bader charge (e)
CuN ₄ /CoN ₂ P ₂ @NPC 	Cu	0.925
	Co	0.373
	N1	-1.134
	N2	-1.119
	N3	-1.473
	N4	-1.469
	N5	-1.166
	N6	-1.040
	P1	1.50
	P2	1.50
CuN ₄ /CoN ₃ P ₁ @NPC 	Cu	0.870
	Co	0.555
	N1	-1.213
	N2	-1.153
	N3	-0.612
	N4	-1.557
	N5	-0.677
	N6	-1.128
	N7	-1.088
	P1	1.622
CuN ₄ /CoN ₄ @NPC 	Cu	0.939
	Co	0.849
	N1	-1.204
	N2	-1.170
	N3	-0.492
	N4	-0.543
	N5	-0.796
	N6	-0.784
	N7	-1.166
	N8	-1.184

Table S5. Aerobic oxidative coupling-dehydrogenation cascade reaction of benzyl alcohol and 2'-hydroxyacetophenone over different catalysts. ^[a]



Entry	Catalyst	Conv. (%)	Selectivity (%)		
			2'-Hydroxy- chalcone	Flavanone	Flavone
1	–	10.1	48.5	–	–
2 ^[b]	CuN ₄ /CoN ₂ P ₂ @NPC	3.3	87.9	–	–
3	CuN ₄ /CoN ₂ P ₂ @NPC	>99	–	–	>99
4	CuN ₄ /CoN ₃ P ₁ @NPC	>99	2.6	15.0	82.4
5	CuN ₄ /CoN ₄ @NPC	>99	7.4	25.5	67.1
6	Cu-ZIF-700	17.8	30.9	–	–
7	Cu-complex@MP-700	29.7	42.4	14.8	–
8	MP-Co-700	35.3	43.9	24.1	6.2
9	MP-700	13.3	75.9	–	–

^[a] Reaction conditions: benzyl alcohol (1 mmol), 2'-hydroxyacetophenone (1.5 mmol), catalyst (total metals, 2 mol% relative to benzyl alcohol), K₂CO₃ (0.2 mmol), *n*-hexanol (4 mL), O₂ (2 bar), 120 °C, 12 h. Conversion and yield were determined by GC-MS based on benzyl alcohol. The products were also confirmed by ¹H-NMR and ¹³C-NMR.

^[b] N₂ (2 bar).

Table S6. The adsorption and disassociation energy of O₂ and the O-O bond length on the samples.

Sample	O ₂ adsorption energy (eV)	O-O bond length (Å)	O ₂ disassociation energy (eV)	Activation energy (eV)
CuN ₄ /CoN ₂ P ₂ @NPC	-1.41	1.31	0.04	0.88
CuN ₄ /CoN ₃ P ₁ @NPC	-1.27	1.30	0.48	1.69
CuN ₄ /CoN ₄ @NPC	-0.82	1.29	1.05	2.36